Angiogenesis (2019) 22:341–354
https://doi.org/10.1007/s10456-018-09660-y

ORIGINAL PAPER

Live imaging of angiogenesis during cutaneous wound healing in adult zebrafish

Chikage Noishiki[1,2] · Shinya Yuge[1] · Koji Ando[3] · Yuki Wakayama[3] · Naoki Mochizuki[3] · Rei Ogawa[2] · Shigetomo Fukuhara[1]

Received: 21 September 2018 / Accepted: 25 December 2018 / Published online: 4 January 2019

Abstract

Angiogenesis, the growth of new blood vessels from pre-existing vessels, is critical for cutaneous wound healing. However, it remains elusive how endothelial cells (ECs) and pericytes (PCs) establish new blood vessels during cutaneous angiogenesis. We set up a live-imaging system to analyze cutaneous angiogenesis in adult zebrafish. First, we characterized basic structures of cutaneous vasculature. In normal skin tissues, ECs and PCs remained dormant to maintain quiescent blood vessels, whereas cutaneous injury immediately induced angiogenesis through the vascular endothelial growth factor signaling pathway. Tortuous and disorganized vessel networks formed within a few weeks after the injury and subsequently normalized through vessel regression in a few months. Analyses of the repair process of injured single blood vessels revealed that severed vessels elongated upon injury and anastomosed with each other. Thereafter, repaired vessels and adjacent uninjured vessels became tortuous by increasing the number of ECs. In parallel, PCs divided and migrated to cover the tortuous blood vessels. ECs sprouted from the PC-covered tortuous vessels, suggesting that EC sprouting does not require PC detachment from the vessel wall. Thus, live imaging of cutaneous angiogenesis in adult zebrafish enables us to clarify how ECs and PCs develop new blood vessels during cutaneous angiogenesis.

Keywords Angiogenesis · Cutaneous wound healing · Endothelial cells · Pericytes · Zebrafish

Introduction

Cutaneous wound healing is a complex and dynamic process by which skin tissue repairs itself after injury, which occurs through a series of interdependent and overlapping phases which include hemostasis, inflammation, proliferation, and maturation phases [1]. During the proliferation phase, fibroblasts deposit extracellular matrix to form granulation tissue, in which endothelial cells (ECs) develop microvascular networks through angiogenesis [2]. During the subsequent maturation phase, new skin tissue is established through remodeling of extracellular matrix and regression of excessive microvasculature. It has been reported that major steps and principles of cutaneous wound healing are conserved not only among adult mammals but in adult zebrafish as well [3]. Thus, zebrafish is a suitable model system for cutaneous wound healing research.

Angiogenesis plays a crucial role in wound healing [2]. It is a complex morphogenetic process whereby ECs sprout from pre-existing blood vessels and migrate to establish neovascular networks [4]. During embryogenesis, angiogenesis

Chikage Noishiki and Shinya Yuge have contributed equally to this work.

Electronic supplementary material The online version of this article (https://doi.org/10.1007/s10456-018-09660-y) contains supplementary material, which is available to authorized users.

✉ Shigetomo Fukuhara
s-fukuhara@nms.ac.jp

[1] Department of Molecular Pathophysiology, Institute of Advanced Medical Sciences, Nippon Medical School, 1-396 Kosugi-machi, Nakahara-ku, Kawasaki, Kanagawa 211-8533, Japan

[2] Department of Plastic, Reconstructive and Aesthetic Surgery, Nippon Medical School, Tokyo, Japan

[3] Department of Cell Biology, National Cerebral and Cardiovascular Center Research Institute, 5-7-1 Fujishirodai, Suita, Osaka 565-8565, Japan

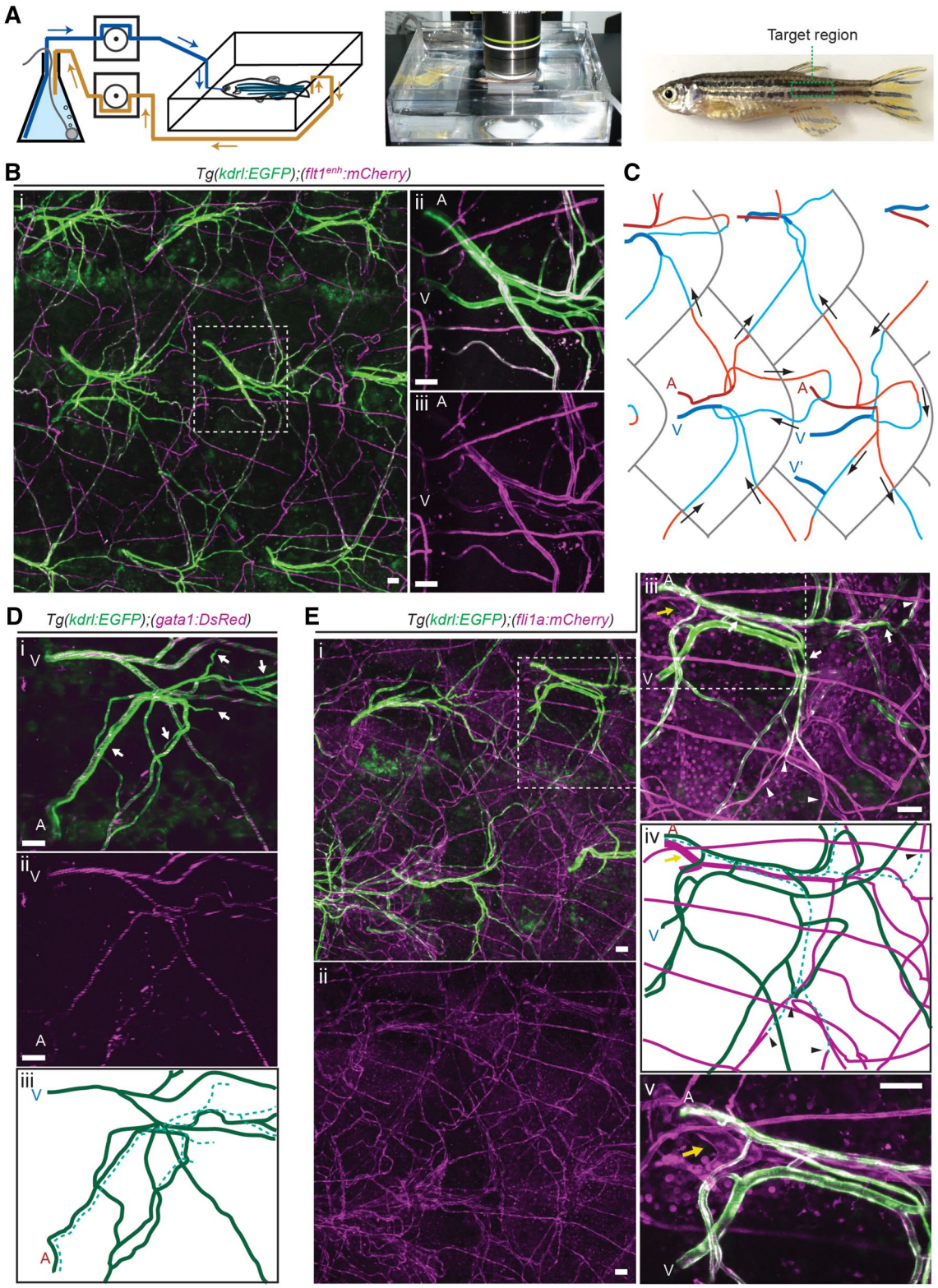

is induced to form stereotypical vascular networks in a developing body in response to both hypoxia and the attractive and repulsive cues released from the surrounding tissues [5, 6]. In contrast, most blood vessels in the body become quiescent in adults. However, angiogenesis is reinitiated by tissue hypoxia during wound healing or in diseases such as cancer, arthritis, diabetic retinopathy, and macular degeneration [4, 6]. Vascular endothelial growth factor (VEGF),

◂**Fig. 1** Cutaneous vasculature in adult zebrafish. **a** Schematic representation of our live-imaging system for adult zebrafish. Imaged region of cutaneous vasculature in adult zebrafish is indicated by the dotted square on the right image. **b** Confocal stack fluorescence images of cutaneous vasculature in the trunk of *Tg(kdrl:EGFP);(flt1*^{enh}*:mCherry)* adult zebrafish. Merged image of *kdrl:EGFP* (green) and *flt1*^{enh}*:mCherry* (magenta) (i). The boxed area in (i) is enlarged to the right where the merged image (ii) and the *flt1*^{enh}*:mCherry* image (iii) are shown. **c** Tracing of cutaneous blood vessels in the trunk of adult zebrafish. Red line, arteries; blue line, veins; gray line, margin of scales; "A" sites where arteries emerge from the muscle layer; "V" or "V'" sites where veins emerge from the muscle layer. Arrows indicate the direction of blood flow. **d** Confocal stack fluorescence images of cutaneous vasculature in the trunk of *Tg(kdrl:EGFP);(gata1:DsRed)* adult zebrafish. Merged image of *kdrl:EGFP* (green) and *gata1:DsRed* (magenta) (i) and the *gata1:DsRed* image (ii). Tracing of cutaneous vasculature as observed in (i) (iii). In (iii), green solid line, *kdrl:EGFP*-positive blood vessels; dotted green line, the vessels which do not contain *gata1:DsRed-positive* erythrocytes. "A" and "V" indicate the sites where arteries and veins emerge from the muscle layer, respectively. Arrows indicate the vessels which do not contain *gata1:DsRed*-positive erythrocytes. **e** Confocal stack fluorescence images of cutaneous vasculature in the trunk of *Tg(kdrl:EGFP);(fli1a:mCherry)* adult zebrafish. The merged image of *kdrl:EGFP* (green) and *fli1a:mCherry* (magenta) (i) and the *fli1a:mCherry* image (ii). The boxed area in (i) is enlarged in (iii). Tracing of cutaneous vasculature as observed in (iii) (iv). The boxed area in (iii) is enlarged (v). In (iv): green solid line, *kdrl:EGFP* and *fli1a:mCherry* double-positive blood vessels; dotted green line, *kdrl:EGFP* and *fli1a:mCherry* double-positive vessels that do not contain erythrocytes; solid magenta line, *fli1a:mCherry*-positive vessels that do not contain erythrocytes. Arrows indicate the *kdrl:EGFP* and *fli1a:mCherry* double-positive vessels that do not contain erythrocytes. Arrowheads indicate the boundary between the *kdrl:EGFP* and *fli1a:mCherry* double-positive vessels and the *fli1a:mCherry*-positive vessels. Scale bars: 50 µm

produced by hypoxic tissues, induces activation of ECs to initiate angiogenesis. Angiopoietin (Ang)-2 released by activated ECs is thought to induce detachment of pericytes (PCs) from the vascular wall, thereby facilitating EC sprouting [7–12].

Recently, significant advances in fluorescence-based bioimaging technology have been made, which have greatly contributed to the progress of research in the field of medical and life sciences. Accordingly, this technology has been applied to study the mechanism of angiogenesis in zebrafish embryos, which is made possible by their transparency [13, 14]. Fluorescence-based live imaging of zebrafish embryos allows us to visualize developmental angiogenesis in living animals, thereby contributing to our understanding of the molecular and cellular mechanisms of developmental angiogenesis. This has the potential to help elucidate the largely unknown mechanisms of how angiogenesis is induced by tissue hypoxia during wound healing or in diseases.

In this study, we set up a live-imaging system to visualize angiogenesis in response to cutaneous wounding in adult zebrafish. By exploiting this system, we characterized basic structures of cutaneous vasculature in adult zebrafish and showed how skin injury induces cutaneous angiogenesis and how the ECs and PCs form neovascular networks in the wounded skin.

Materials and methods

Plasmids

A cDNA fragment encoding mCherry was amplified by PCR using the pmCherry-C1 plasmid (Clonetech, Takara Bio Inc.) as a template and subcloned into the pTolfli1 vector [15] to construct the pTol2-fli1:mCherry plasmid. The Tol2 vector system was kindly provided by K. Kawakami (National Institute of Genetics, Japan) [16].

Zebrafish husbandry

Zebrafish were bred and maintained as previously described [15]. Animal experiments were approved of and performed in accordance with the guidelines established by the animal committees of the National Cerebral and Cardiovascular Center and the Nippon Medical School.

Transgenic zebrafish lines

Tol2 transposase mRNAs were in vitro transcribed with SP6 RNA polymerase from NotI-linearized pCS-TP vector using the mMESSAGE mMACHINE kit. To generate the *Tg(fli1a:mCherry)*^{ncv501} zebrafish line, the pTol2-fli1:mCherry plasmid (25 pg) was microinjected along with Tol2 transposase RNA (25 pg) into one-cell stage embryos of the wild-type strain, AB. The embryos showing transient expression of mCherry in the vasculature were selected, raised to adulthood, and crossed with wild-type AB to identify germline transmitting founder fishes.

Tg(kdrl:eGFP)^{s843} and *Tg(gata1:DsRed)*^{sd2} fish were provided by Stainier (Max Planck Institute for Heart and Lung Research) [17]. Generation of *Tg(flt1*^{enh}*:mCherry)*^{ncv30} and *TgBAC(pdgfrb:mCherry)*^{ncv23} zebrafish lines were previously described [18, 19]. Throughout the text, all transgenic lines used in this study are simply described without their line numbers.

Live imaging of adult zebrafish

We set up a live-imaging system for adult zebrafish by modifying the protocol previously described by Xu et al. [20]. Schematic representation of our live-imaging system for adult zebrafish is shown in Fig. 1a. Fish water containing anesthetic was stored in a 500-ml flask, which was kept in a water bath to maintain a constant temperature (28 °C), and delivered to a fish chamber (plastic case:

100 mm × 100 mm × 29 mm, AS ONE) via a silicone tube (size: 5–3, ATTO) using a peristatic pump (ATTO). The adult zebrafish mounted in the chamber was orally perfused with the fish water containing anesthetic using an Intramedic polyethylene tube (inner diameter: 0.86 mm; outer diameter: 1.27 mm, BD). Excess water in the fish chamber was removed and returned to the flask via a silicone tube using another peristatic pump. This allowed for the fish water to be circulated inside the system during live imaging.

Adult male zebrafish were anesthetized with 0.06% 2-phenoxyethanol (Sigma-Aldrich) in fish water, transferred to the fish chamber, and immobilized by covering the trunk and tail regions, except for the pectoral fins and the injured area with 1.5% low-melting-point agarose gel (Thermo Fisher Scientific). After inserting the polyethylene tube into the mouth of fish, the fish were continuously orally perfused with fish water containing 0.035–0.04% 2-phenoxyethanol at the speed of 5.5–6.0 ml/min, and subjected to cutaneous wounding and live imaging. For recovery from anesthesia, the fish were perfused with fish water without 2-phenoxyethanol for 5–10 min.

Confocal Z-stack images were obtained using a FluoView FV1200 or FV3000 confocal upright microscope (Olympus) equipped with a water-immersion 10× (UMPlanFL N, 0.30 NA) and 20× (XLUMPlanFL N, 1.00 NA) objective lens. Lasers with excitation wavelengths of 473 nm and 559 nm were employed. Fluorescence images were acquired sequentially at 473 nm and 559 nm wavelengths to avoid cross-detection of the fluorescent signals. Obtained confocal images were processed using Volocity 3D Imaging analysis software (PerkinElmer) and Photoshop software (Adobe Systems Co.).

Cutaneous wounding in zebrafish

To injure the skin of adult zebrafish, we removed 4–6 scales and introduced wounds onto the flank of adult zebrafish using fine forceps (Dumont No. 5) under a microscope equipped with a × 10 dry (Plan, 0.25 NA) or × 20 water-immersion (UMPlanFL N, 0.50 NA) objective lens. This wounding procedure resulted in loss of the scales and most of the epidermal and dermal cells, but did not damage the subcutaneous adipocytes and underlying muscle tissue. We additionally injured a single capillary in the skin of adult zebrafish using a Terumo Needle 20G under a confocal microscope.

Quantifications

Tortuosity index of blood vessels was calculated as previously described [21]. Briefly, we measured the geodesic distance (L_G) and Euclidean distance (L_E) between both ends of vessel segment. Then, we multiplied the ratio of L_G to L_E by the number of times the vessel changes direction with a degree of < 160°.

To quantify the sprouting, bifurcation, and pruning of blood vessels during cutaneous angiogenesis, we counted the number of events that occurred between sequential time points in the imaged area (4×10^5 μm^2).

Results

Structure of cutaneous vasculature in adult zebrafish

To investigate the mechanism underlying wound angiogenesis, we utilized an intubation-based anesthesia protocol for adult zebrafish, as shown in Fig. 1a. Using this system, we visualized cutaneous vascular structures by imaging the *Tg(kdrl:EGFP);(flt1^{enh}:mCherry)* line, in which ECs and arterial ECs were labeled by EGFP and mCherry fluorescence, respectively (Fig. 1b, c). We additionally observed circulating erythrocytes using the *Tg(kdrl:EGFP);(gata1:DsRed)* line to identify blood vessels (Fig. 1d). Furthermore, we imaged the pan-endothelial *Tg(fli1a:mCherry)* transgenic line to analyze cutaneous vasculature (Fig. 1e). An artery and vein extended from the muscle layer around the center of each scale (Fig. 1b, c). Additional veins emerged from the muscle layer covered by some scales (Fig. 1c). The artery often branched into two or three capillaries, which were directly returned to the vein next to the original artery or connected to the veins located within the neighboring scales (Fig. 1b, c).

In addition to blood vessels, the vascular networks, which do not contain circulating erythrocytes, were formed in the skin of adult zebrafish (Fig. 1b–e). In such networks, the vessels positive for *kdrl:EGFP, flt1^{enh}:mCherry* and *fli1a:EGFP* emerged from the muscle layer and extended along the arteries (Fig. 1b–e). After separating from the arteries, they became double-positive for *flt1^{enh}:mCherry* and *fli1a:mCherry* and were connected to the *fli1a:mCherry*-positive vessel networks aligned along the scale surface and the margin of posterior scale (Fig. 1b–e). Then, the *fli1a:mCherry*-positive vessels in the scale converged on the large diameter vessels which, in turn, entered the muscle layers around an artery and vein pair (Fig. 1e). At present, it is unclear whether the cutaneous vessel networks which do not contain circulating erythrocytes correspond to a lymphatic system or a secondary circulation system, which was previously identified in bony fish [22] (see the "Discussion" section).

We also analyzed PCs covering the cutaneous vasculature by imaging the *TgBAC(pdgfrb:mCherry);Tg(kdrl:EGFP)* and *TgBAC(pdgfrb:mCherry);Tg(fli1a:EGFP)* lines (Supplementary Fig. 1). The *pdgfrb:mCherry*-positive PCs were

found to cover the most of cutaneous blood vessels. In addition, the most cutaneous vessels, which do not contain circulating erythrocytes, were covered by the *pdgfrb:mCherry*-positive cells, although it remains unclear whether these cells are the PCs.

Among the cutaneous vasculature, we focused on the blood vessels and their surrounding PCs in this study.

Induction of angiogenesis by cutaneous wounding

To better understand how angiogenesis occurs during cutaneous wound healing, we first analyzed blood vessels in the normal skin tissues. We observed ECs and PCs present in the capillaries by imaging the *TgBAC(pdgfrb:mCherry);Tg(kdrl:EGFP)* fish line, which labels the ECs and PCs with EGFP and mCherry fluorescence, respectively (Fig. 2a). ECs and PCs existed within the capillaries at average intervals 47.5 and 80.3 μm, respectively (Fig. 2a, b). The ratio of PCs to ECs (PC/EC) in the capillaries was 0.61 ± 0.13 (Fig. 2c). In addition, the number and position of ECs and PCs in the capillaries remained almost unchanged for approximately 2 months (Fig. 2a). Time-lapse imaging of normal skin vasculature for 17 h showed no movement of ECs in the normal skin capillaries (Supplementary Movie S1). These results reveal that ECs and PCs remain dormant in the normal skin, thereby maintaining the quiescent vessels.

To investigate the impact of tissue injury on quiescent cutaneous vasculature, we introduced wounds onto the flank of adult *Tg(kdrl:EGFP)* zebrafish using fine forceps and time-lapse imaged cutaneous wound angiogenesis (Fig. 2d; Supplementary Movie S2). Cutaneous wounding immediately evoked angiogenesis. These findings suggest that cutaneous wounding immediately activates dormant ECs to induce angiogenesis.

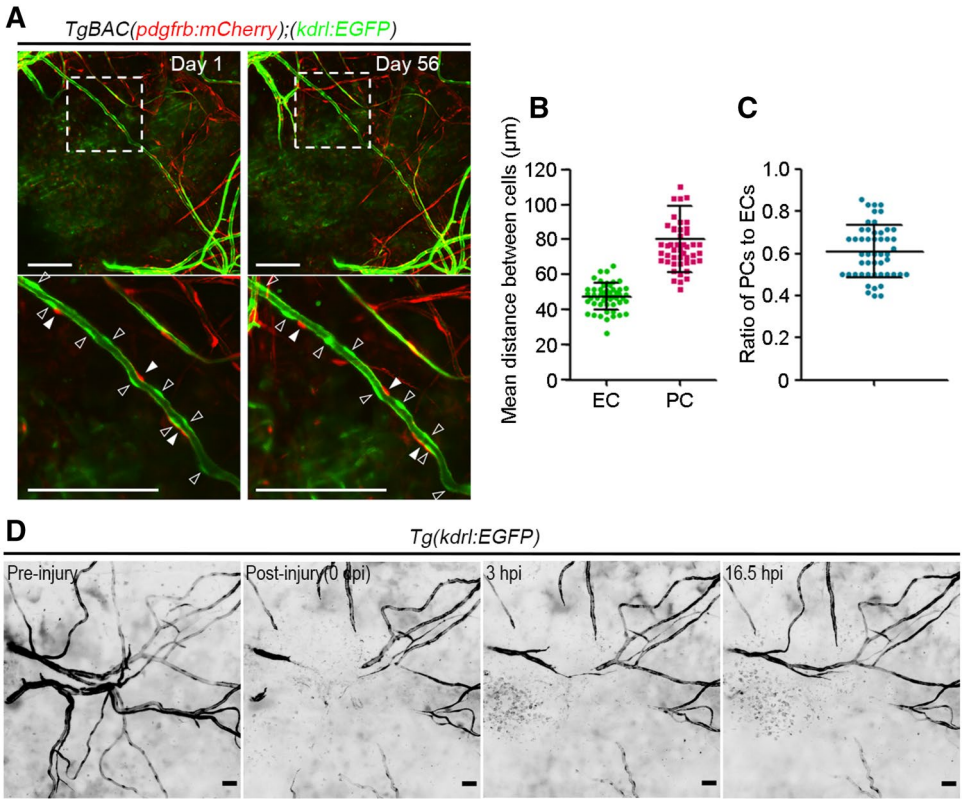

Fig. 2 Induction of angiogenesis by cutaneous injury. **a** Confocal stack fluorescence images of cutaneous blood vessels in the trunk of *TgBAC(pdgfrb:mCherry);Tg(kdrl:eGFP)* adult zebrafish. Images in the left and right columns show cutaneous vasculature in the same region on the 1st and 56th day, respectively. Merged images of *pdgfrb:mCherry* (red) and *kdrl:eGFP* (green). The boxed areas are enlarged to the bottom. Open and closed arrowheads label the positions of ECs and PCs, respectively. **b** Mean distance between ECs and between PCs in the cutaneous blood vessels as observed in (**a**). Each dot represents the mean distance between ECs or PCs in the individual vessels ($n = 50$). Error bars indicate means ± s.d. **c** The ratio of PCs to ECs in the cutaneous blood vessels as observed in a. Each dot represents the ratio of PCs to ECs in the individual vessels ($n = 50$). Error bars indicate means ± s.d. In (**b, c**), the unbranched parts of cutaneous capillaries (230–600 μm length) were analyzed. **d** Time-lapse confocal images of the cutaneous blood vessels in the trunk of *Tg(kdrl:EGFP)* adult zebrafish. 3D-rendered confocal images before (pre-injury) and after (post-injury) the injury and its subsequent time-lapse images with the elapsed time (h) at the top. Scale bars: 100 μm (**a, d**); 50 μm (**e**)

Angiogenic process during cutaneous wound healing

To investigate how new blood vessels are established in the damaged skin, we introduced wounds onto the flank of adult *Tg(kdrl:EGFP)* zebrafish and monitored time-dependent changes in the blood vessel structures during cutaneous wound angiogenesis (Figs. 3, 4; Supplementary Fig. 2). This wounding procedure resulted in loss of the scales and most of epidermal and dermal cells, but did not damage the subcutaneous adipocytes and underlying muscle tissue. At 2 days post-injury (dpi), elongation of the injured blood vessels was observed (Fig. 3). In addition, some blood vessels became tortuous and began to sprout new branches (Figs. 3, 4a, b; Supplementary Fig. 3a). At 4 dpi, tortuosity of the blood vessels dramatically increased (Figs. 3, 4a; Supplementary Fig. 3a). Furthermore, numerous new vessels were sprouted from the tortuous vessels and some of them underwent bifurcation, leading to formation of many vessel branches (Figs. 3, 4b–d; Supplementary Fig. 3b, c). Then, some branches were connected to the neighboring blood vessels to form a number of small vascular loops, as evidenced by an increase in the number of branching points (Figs. 3, 4e; Supplementary Fig. 3b, c). As a result, dense, disorganized, and complex vascular networks were formed in the wounded cutaneous tissues at 6 dpi (Fig. 3). At 6–14 dpi, tortuosity of the blood vessels gradually decreased, and excessive blood vessels started to regress (Figs. 3, 4a, f). At 42 dpi, the tortuous blood vessels became more linear, and pruning of excessive blood vessels further proceeded (Figs. 3, 4a, f; Supplementary Fig. 3d). As a result, new blood vessels in the injured tissue became more organized and established vascular networks resembling those in the pre-injured tissue (Fig. 3). After that, the vascular network structures remained almost unchanged until 170 dpi (Fig. 3), suggesting that ECs in the new blood vessels reached a quiescent state around

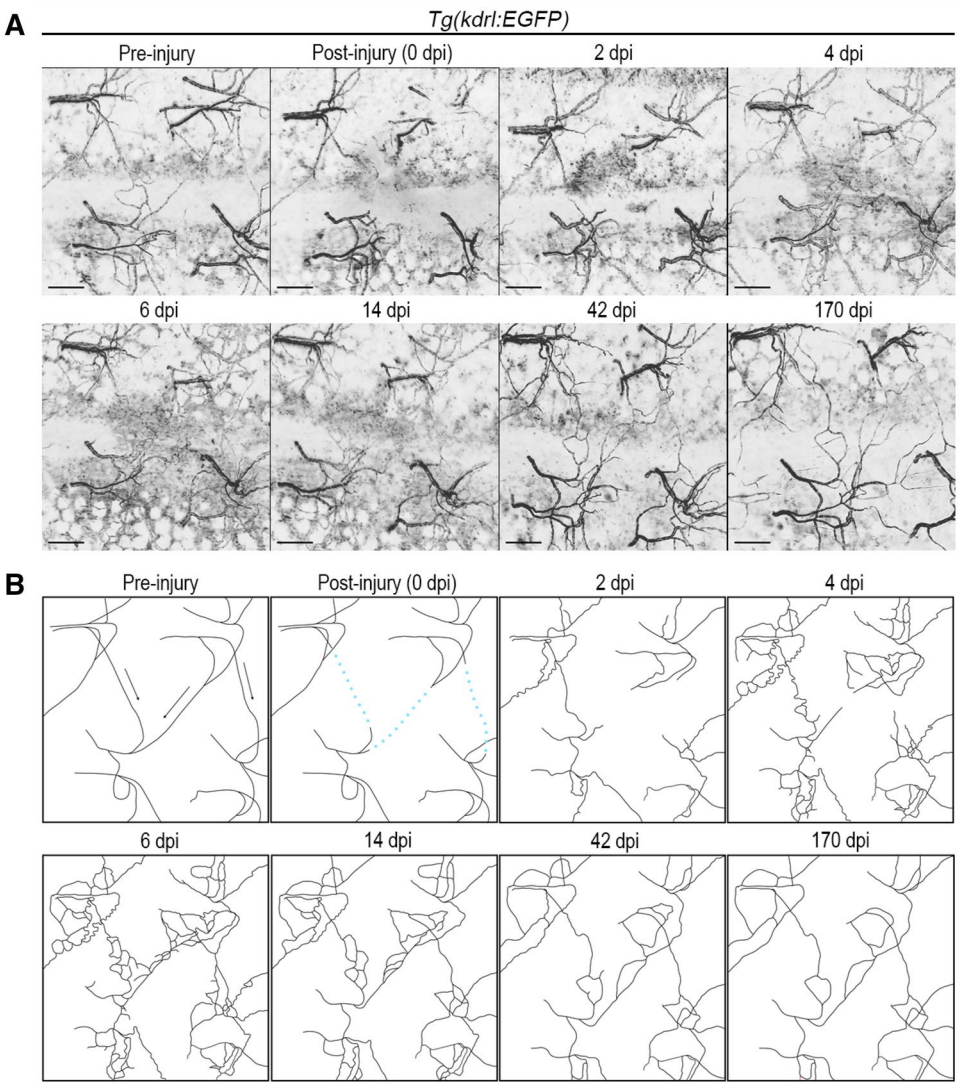

Fig. 3 The process of angiogenesis during cutaneous wound healing. After injuring cutaneous tissue in the trunk of *Tg(kdrl:eGFP)* adult zebrafish, angiogenic process during cutaneous wound healing was observed until 170 dpi. **a** Confocal stack images of the cutaneous tissue before (pre-injury) and after (post-injury) the injury and at the subsequent timepoints indicated at the top. Scale bars: 200 μm. **b** Tracing of blood vessels during cutaneous wound healing as observed in (**a**). Arrows indicate the direction of blood flow. Dotted blue lines show the injured blood vessels

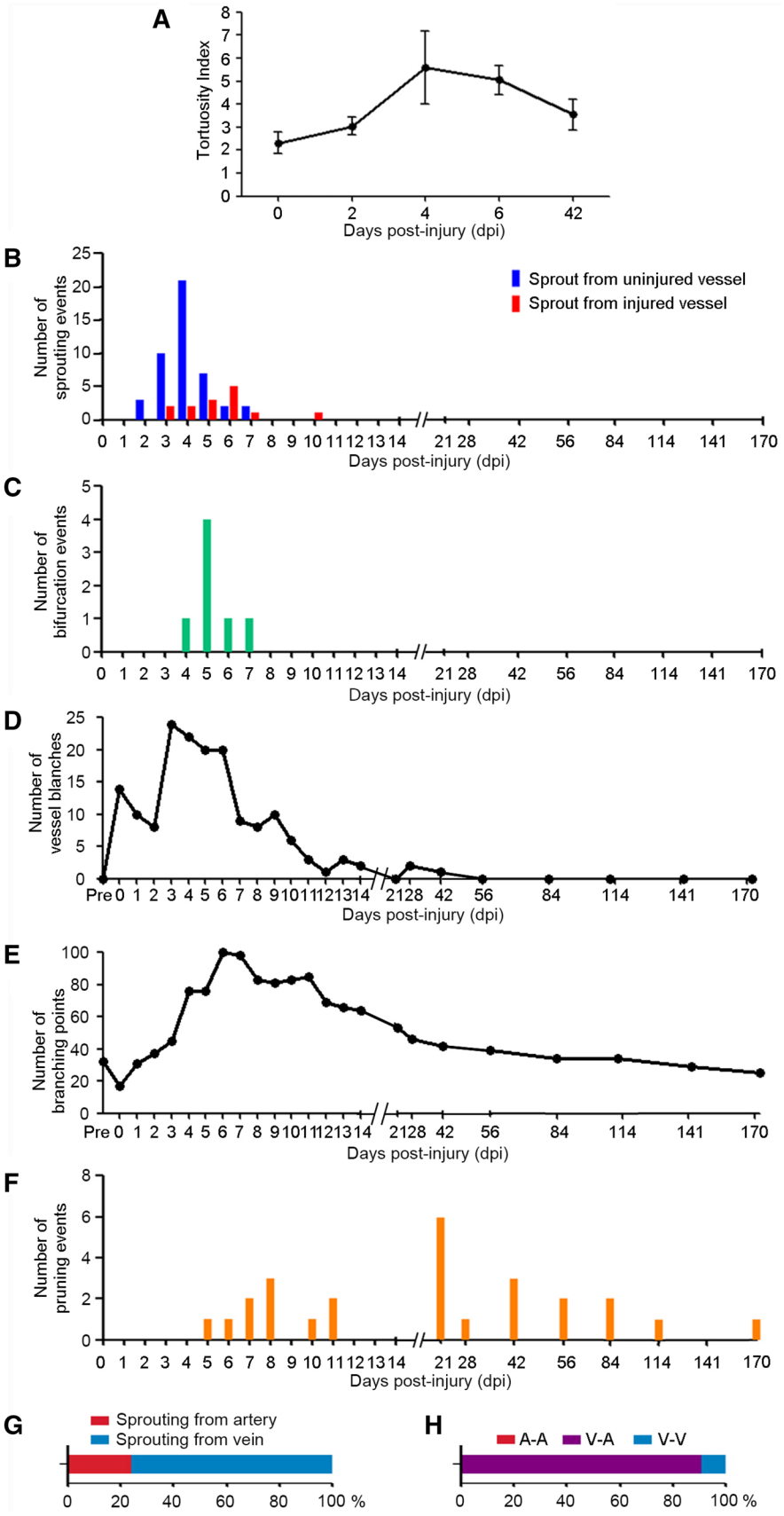

Fig. 4 Quantitative analysis of angiogenesis during cutaneous wound healing as observed in Fig. 3. **a** Tortuosity of blood vessels in the injured tissue at the indicated time points. Vessel segments randomly selected from the imaged area (4×10^5 μm^2) at each time point were analyzed to quantify the tortuosity index as described in "Materials and methods." Data are shown as means ± s.e.m. ($n = 9$). **b** Number of sprouting events from the uninjured (blue bars) and injured (red bars) blood vessels in the injured tissue at the indicated time points. Number of vessel bifurcation events (**c**), vessel branches (**d**), vessel branching points (**e**), vessel pruning events (**f**) in the injured tissue at the indicated time points. **g** Percentage of sprouting events from the arteries and the capillaries on the arterial side (red) and those from veins and the capillaries on the venous side (blue) ($n = 58$). **h** Percentage of anastomotic events between arteries (red), those between an artery and a vein (purple), and those between veins (blue) ($n = 11$)

42 dpi. Similar results were obtained from another set of experiments (Supplementary Fig. 2). These findings indicate that cutaneous wounding immediately and actively induces angiogenesis to form dense and disorganized vascular networks within a few weeks after the injury, and subsequently those vessels become normalized through regression of excess vascular networks by 1–2 months after the injury.

We also investigated whether sprouting occurs from both arteries and veins or only from either type of vessels. To this end, we counted the number of vessels sprouting from the arteries and the capillaries in the arterial side and those from veins and the capillaries in the venous side. Approximately 76% of vessel branches were sprouted from the veins or the capillaries on the venous side, and mainly connected to capillaries on the arterial side (Fig. 4g, h). On the other hand, approximately 24% of vessel branches were sprouted from the arteries or the capillaries on the arterial side, and connected to the capillaries on the venous side (Fig. 4g, h). These results suggest that venous ECs are more active than arterial ECs during cutaneous angiogenesis.

We next investigated whether VEGF signaling is required for induction of cutaneous wound angiogenesis by treating the *Tg(kdrl:EGFP)* fish with the VEGF receptor inhibitor, Ki8751. In the uninjured skin, blood vessel structures and blood circulation remained unchanged even in the presence of Ki8751 (Fig. 5a). In clear contrast, treatment with Ki8751 severely blocked the induction of cutaneous wound angiogenesis, which is the sprouting and bifurcation of blood vessels and the emergence of tortuous blood vessels (Fig. 5b–e). However, cutaneous angiogenesis was immediately induced by removal of Ki8751 from the environment (Fig. 5b–e). These results indicate that VEGF signaling is required for induction of angiogenesis during cutaneous wound healing, but not for maintenance of quiescent blood vessels in the skin of adult zebrafish.

Observation of ECs and PCs during cutaneous angiogenesis

It is currently thought that PCs detach from the wall of blood vessels upon induction of angiogenesis, thereby allowing ECs to sprout in response to angiogenic growth factors [7–12]. To confirm this concept, we decided to analyze ECs and PCs during cutaneous angiogenesis. To this end, we injured a single capillary in the skin of the *TgBAC(pdgfrb:mCherry);Tg(kdrl:EGFP)* fish line, and monitored the repair process by visualizing ECs and PCs in the injured blood vessels and adjacent uninjured vessels (Fig. 6; Supplementary Fig. 4). Blood vessels immediately elongated upon injury and anastomosed with each other at approximately 2–3 dpi (Fig. 6a). At this time, the repaired blood vessels consisted of almost same number of ECs and PCs as in the pre-injured ones (Fig. 6b). After that, however, the numbers of ECs and PCs in the repaired vessels increased, while the ratio of PCs to ECs remained constant, and reached approximately 1.8-fold of the number in the pre-injured vessels at 7 dpi (Fig. 6a, b). As a result, the PC-covered tortuous blood vessels appeared, and were maintained until approximately 14 dpi (Fig. 6a–c). Subsequently, they became normalized by gradually decreasing the number of ECs and PCs over time (Fig. 6a–c). In addition, injury of single blood vessel additionally affected the adjacent uninjured vessels (Fig. 6a, c, d). In those blood vessels, the numbers of ECs and PCs likewise started to increase from 2 dpi and reached a plateau at 6–7 dpi (approximately 1.4- and 1.6-fold increases in the number of ECs and PCs compared with those before the injury, respectively), which resulted in transformation of linear blood vessels to the PC-covered tortuous vessels (Fig. 6a, c, d). Subsequently, the PC-covered tortuous blood vessels became normalized by gradually decreasing the number of ECs and PCs (Fig. 6a, c, d). These findings reveal that both ECs and PCs increase at the early stage of cutaneous angiogenesis and decrease during the vessel regression at the late stage.

This result conflicts with the current concept that induction of angiogenesis induces PC detachment from the vessel wall to facilitate EC sprouting. Therefore, we carefully analyzed the relationship between the site of EC sprouting and the position of PCs, and found that ECs sprouted from the blood vessels regardless of the position of PCs (Fig. 7a, b). Average distance from the sprouting site of ECs to the PC position was 20.4 ± 13.7 μm (Fig. 7b). However, more than 20% of ECs were found to sprout from the vessel sites where PCs exist within 5 μm (Fig. 7b). These findings suggest that detachment of PCs from the vessel wall is not essential for EC sprouting during cutaneous wound angiogenesis.

Division and migration of PCs on blood vessels during cutaneous angiogenesis

Finally, we investigated how PCs emerge to cover the blood vessels during cutaneous angiogenesis. For this purpose, we imaged the PCs and ECs in the wounded skin of the *TgBAC(pdgfrb:mCherry);Tg(kdrl:EGFP)* fish line every 3 h to track the behavior of PCs. We frequently observed division and migration of PCs on the blood vessels. For example, a PC covering the tortuous vessel divided into two daughter PCs, which in turn moved in the opposite direction (Fig. 8a). In addition, PCs surrounding the injured blood vessel divided during the repair process (Fig. 8b). Furthermore, PCs located at the base of a sprouting blood vessel migrated toward the tip and divided during vessel elongation (Fig. 8c; Supplementary Fig. 5). These results suggest that PCs increase in number by cell division and migrate to cover the new blood vessels and the tortuous blood vessels during cutaneous wound angiogenesis.

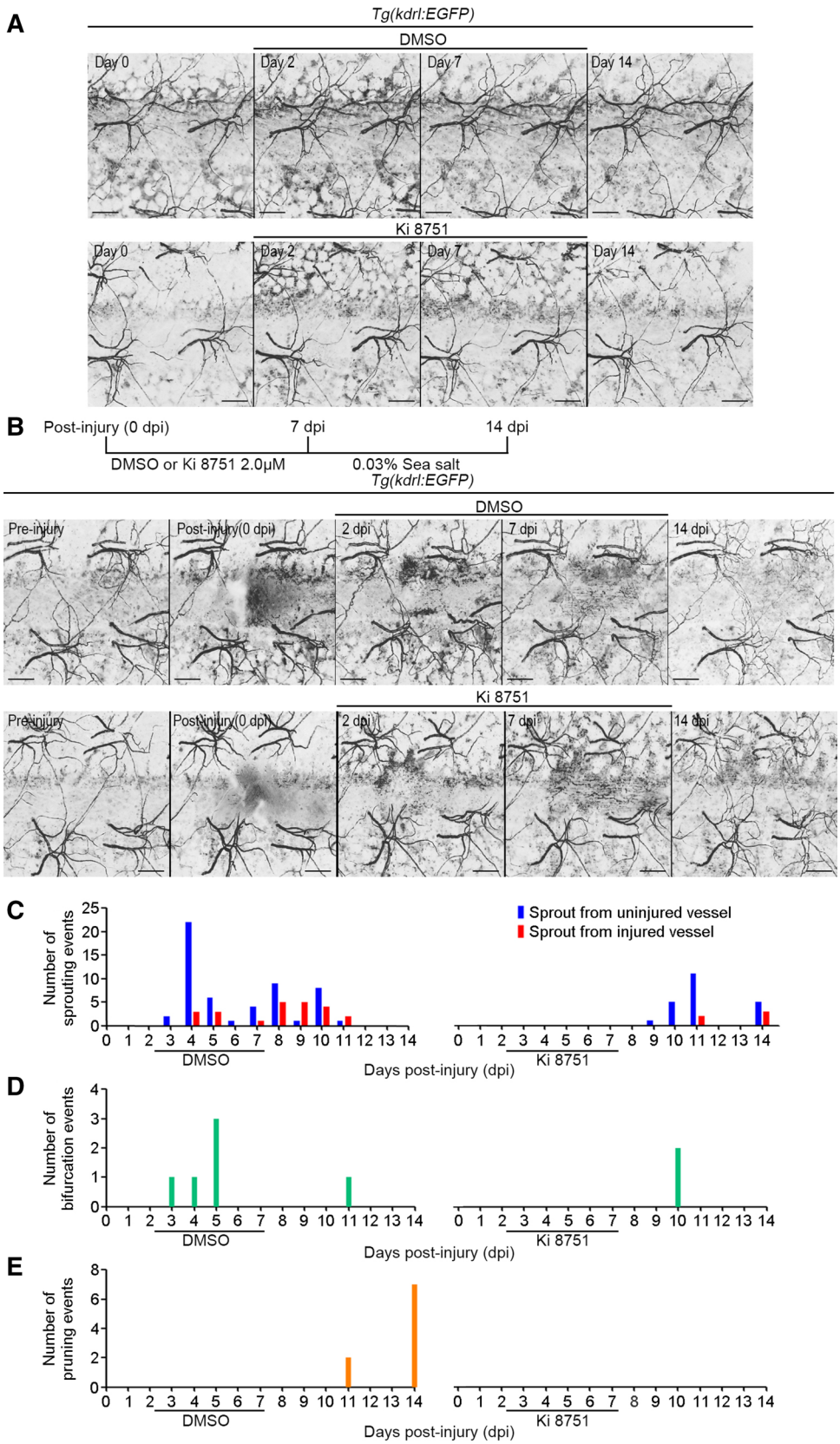

Fig. 5 Requirement of VEGF signaling for cutaneous wound angiogenesis. **a** The *Tg(kdrl:eGFP)* adult zebrafish were incubated in the fish water containing vehicle (DMSO, upper) or 2 μM Ki8751 (lower) for 7 days, and subsequently kept in the fish water for additional 7 days. Confocal stack GFP images of the cutaneous tissue at the timepoints indicated at the top. **b** After injuring cutaneous tissue, the *Tg(kdrl:eGFP)* adult zebrafish were incubated in the fish water containing vehicle (DMSO, upper) or 2 μM Ki8751 (lower) until 7 dpi, and subsequently kept in the fish water for additional 7 days. Confocal stack GFP images of the cutaneous tissue before (pre-injury) and after (post-injury) the injury and at the subsequent timepoints indicated at the top. **c** Number of sprouts from the uninjured (blue bars) and injured (red bars) blood vessels during cutaneous wound angiogenesis in the presence of DMSO (left) and Ki8751 (right) as observed in (**b**). **d** Number of vessel bifurcations during cutaneous wound angiogenesis in the presence of DMSO (left) and Ki8751 (right) as observed in (**b**). **e** Number of vessel regression during cutaneous wound angiogenesis in the presence of DMSO (left) and Ki8751 (right) as observed in (**b**). Scale bars: 200 μm (**a, b**)

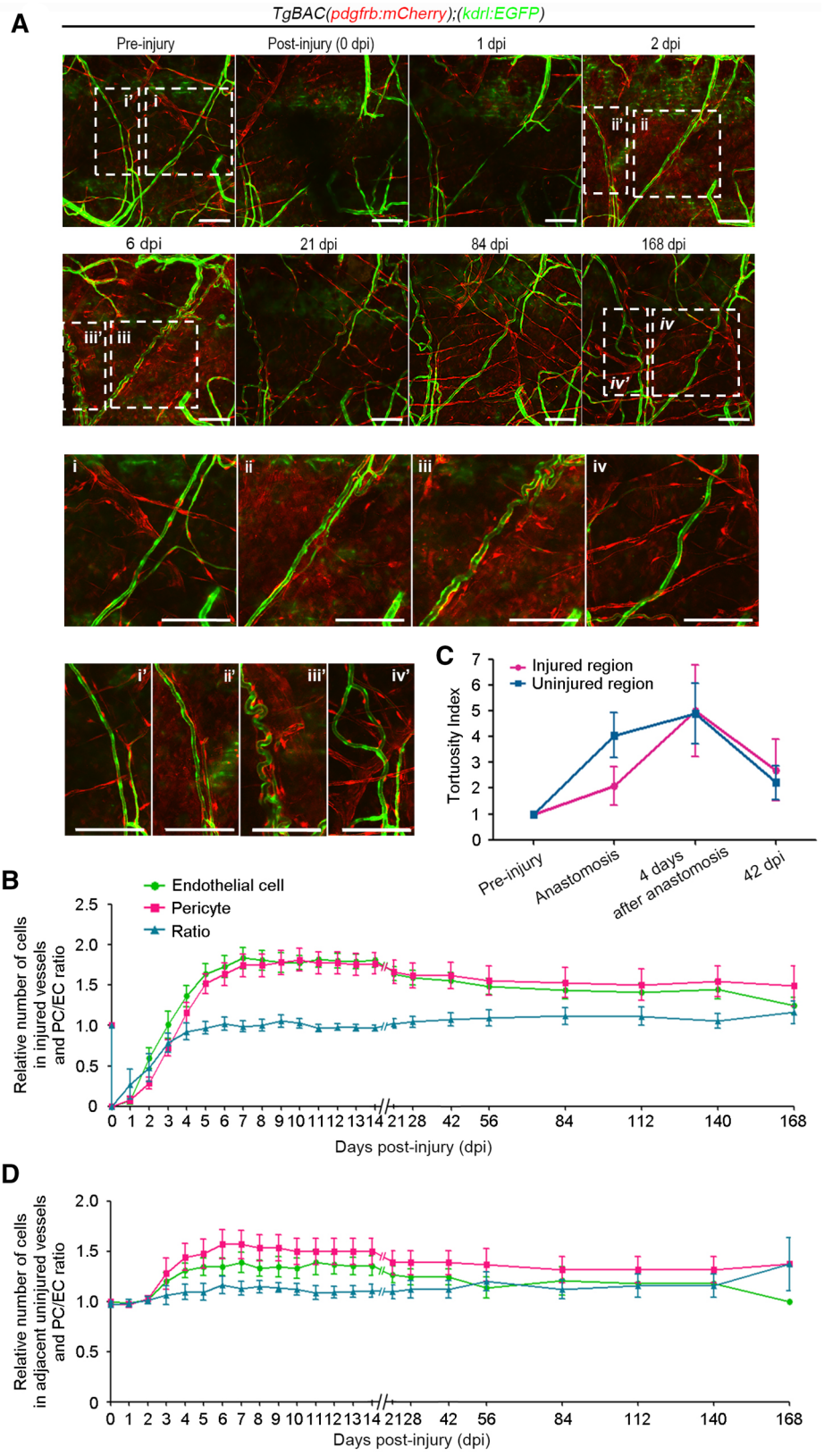

Fig. 6 ECs and PCs during repair of the injured blood vessel. A single blood vessel in the cutaneous tissue of *TgBAC(pdgfrb:mCherry);Tg(kdrl:EGFP)* adult zebrafish was injured as described in Supplementary Fig. 3, and subsequent repair processes were observed until 168 dpi. **a** Confocal stack fluorescence images before (pre-injury) and after (post-injury) injury and at the subsequent timepoints indicated at the top. The merged images of *pdgfrb:mCherry* (red) and *kdrl:EGFP* (green). The boxed areas indicated by i–iv and i′–iv′ indicate the injured and uninjured vessels, and are enlarged to the third and fourth rows, respectively. Scale bars: 100 μm. **b** Relative number of ECs (green) and PCs (red) and relative ratio of PCs to ECs (blue) in injured blood vessels were analyzed as described in Supplementary Fig. 3. Data at the time points indicated at the bottom are expressed as the fold increase relative to that observed in the pre-injured blood vessels. Data are shown as means ± s.e.m. ($n = 11$). **c** Tortuosity index of injured and adjacent uninjured vessels before injury (pre-injury), at a time when anastomosis of injured vessel occurred (anastomosis), 4 days after the anastomosis occurred (4 days after anastomosis), and 42 dpi (42 dpi) was quantified as described in Materials and methods. Data are shown as means ± s.e.m. ($n = 5$–7). **d** Relative number of ECs (green) and PCs (red) and relative ratio of PCs and ECs (blue) in the adjacent uninjured blood vessels are shown as in (**b**). Data are shown as means ± s.e.m. ($n = 8$)

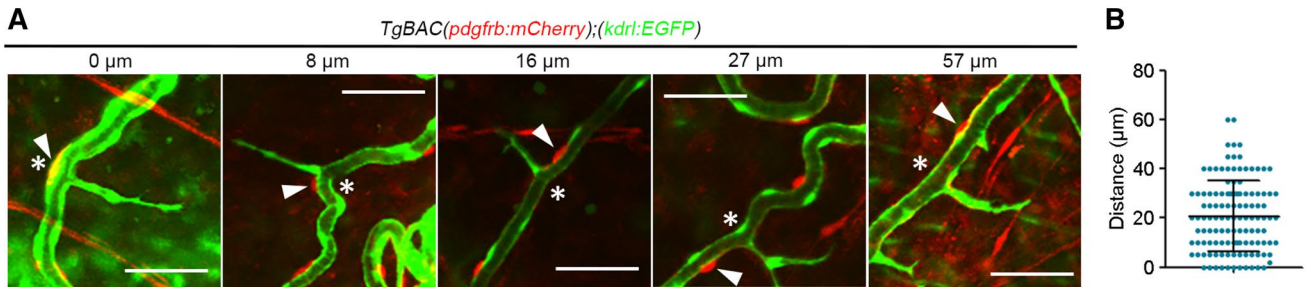

Fig. 7 Positions of ECs and PCs in sprouting blood vessels during cutaneous wound angiogenesis. **a** Confocal stack fluorescence images of blood vessels during cutaneous wound angiogenesis in *TgBAC(pdgfrb:mCherry);Tg(kdrl:EGFP)* adult zebrafish. The merged images of *pdgfrb:mCherry* (red) and *kdrl:EGFP* (green). Asterisks and arrowheads indicate the sprouting site of ECs and the positions of PCs located closest to the sprouting site, respectively. The distance from the EC sprouting site to the PC position is shown at the top. Scale bars: 100 μm. **b** Distance from the sprouting site of ECs to the position of PCs as observed in (**a**). Each dot represents the value in the individual sprouts. Error bars indicate means ± s.d. ($n = 98$)

Discussion

In this study, we imaged the complex and dynamic processes of angiogenesis during cutaneous wound healing in adult zebrafish and showed how skin injury induces cutaneous angiogenesis and how the ECs and PCs form neovascular networks in the wounded skin. Thus, this study provides the basis for understanding the mechanism of cutaneous wound angiogenesis and its role in wound repair.

We have, for the first time, characterized the basic structure of blood vessels in the skin of adult zebrafish, which provides a suitable model system to analyze skin vasculature in living animals. In addition, we identified a type of vessel network which does not contain circulating erythrocytes in the zebrafish skin. Those vessels emerged from the muscle layer and connected to the networks formed along the scale surface and posterior scale margin. Although the vessels on the scales in adult zebrafish have recently been reported as blood vessels [23], we have never observed circulating erythrocytes within these vessels. In addition, more than two decades ago, the secondary circulation system was identified in bony fish [22]. Furthermore, the existence of a functional lymphatic system in zebrafish embryos and adults has been demonstrated [24, 25]. Therefore, further investigations need to be conducted to fully characterize the cutaneous vascular networks in adult zebrafish.

Both ECs and PCs increase during the early stage of cutaneous angiogenesis, leading to the formation of the PC-covered tortuous blood vessels. Formation of tortuous blood vessels is often observed under physiological and pathological angiogenesis [21, 26–29]. Importantly, it has been reported that tortuous vessels appear during the proliferation phase of wound healing and become normalized when the wound heals, as we observed in this study [27]. Recently, Chong et al. have further reported that ECs preferentially sprout from the tortuous microvessels, suggesting that formation of tortuous vessels facilitates EC sprouting to promote wound healing [21]. In this study, we analyzed PC behavior during cutaneous angiogenesis. Unexpectedly, we found that the numbers of ECs and PCs increased in parallel during the early phase of cutaneous angiogenesis, which resulted in the formation of the tortuous blood vessels covered by PCs. These findings conflict with the current concept that PC detachment from the vessel wall is required for efficient EC sprouting [7–12]. We observed that ECs sprouted from the blood vessels regardless of the position of PCs. Thus, the question arose as to why PCs cover the tortuous blood vessels. Because PCs stabilize blood vessels by maintaining EC quiescence [30, 31], they might prevent excessive sprouting of ECs to form the organized blood vessels. In addition, the tortuous blood vessels are known to exhibit increased permeability [21, 32]. Therefore, PCs may additionally suppress the permeability of tortuous blood vessels, because they are known to enhance endothelial barrier function [30, 31]. Consistently, blood vessels lacking coverage of PCs are frequently observed in pathological conditions, such as cancer and diabetic retinopathy, and characterized as tortuous and leaky vessels [10, 30, 33, 34]. As an alternative possibility, PC coverage might facilitate sprouting and elongation of ECs from the tortuous blood vessels because it has been reported that PC-deficiency results in impairment of sprouting angiogenesis [35–37]. Thus, further studies are needed to determine the precise role of PC coverage of tortuous vessels during cutaneous wound angiogenesis.

Induction of cutaneous angiogenesis induces proliferation and migration of PCs to cover the blood vessels. We observed that the number of ECs and PCs changed in parallel during cutaneous angiogenesis, suggesting the regulation of PC proliferation and migration by activated ECs. Indeed, endothelial tip cells express platelet-derived growth factor (PDGF)-B during sprouting angiogenesis [38]. Previous in vitro study also suggested that VEGF induces expression

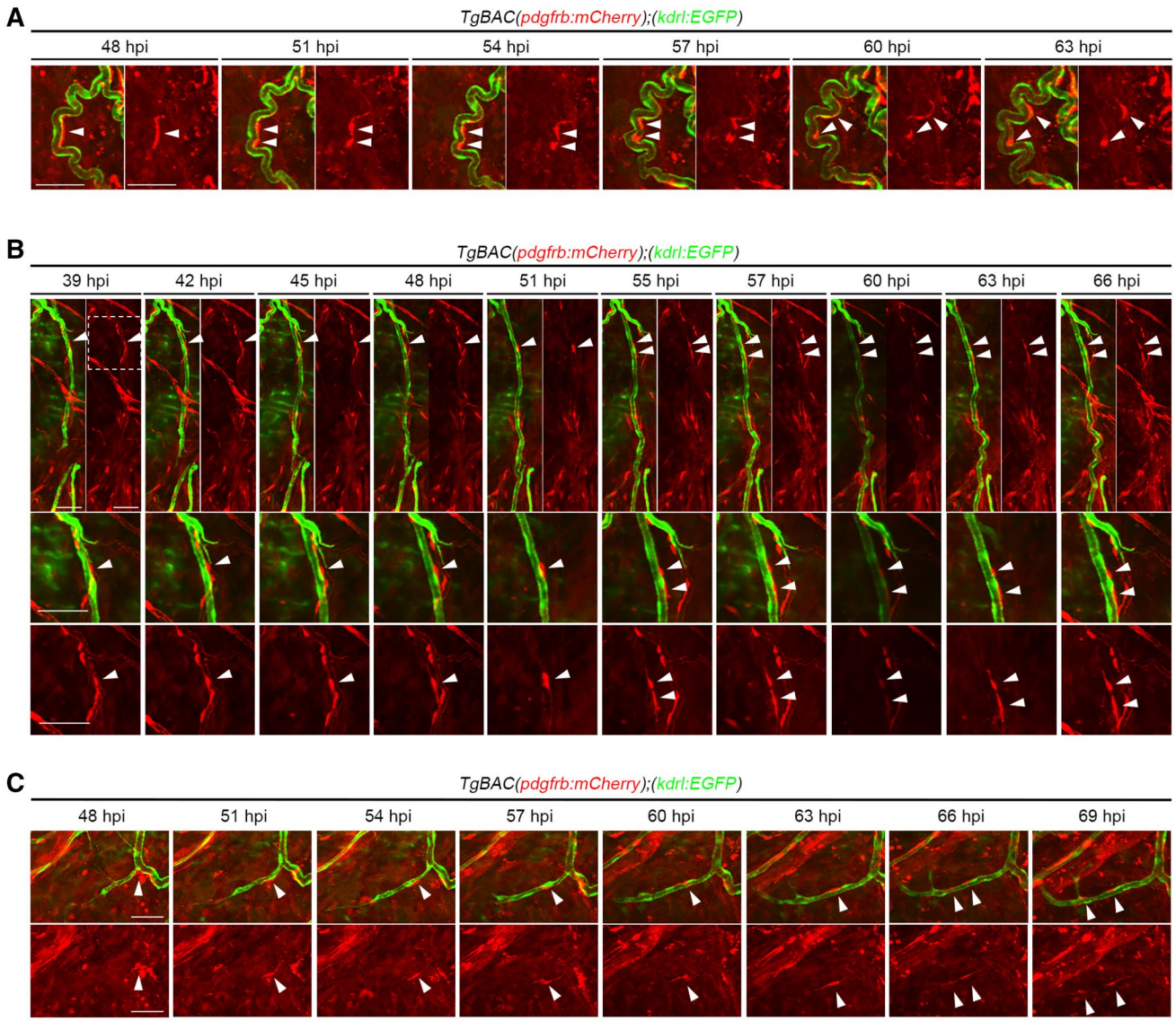

Fig. 8 Division and migration of PCs during cutaneous wound angiogenesis. After injuring cutaneous tissues in the *TgBAC(pdgfrb:mCherry);Tg(kdrl:EGFP)* adult zebrafish, wound angiogenesis was monitored every 3 h to track the PCs. Confocal stack fluorescence images of the tortuous blood vessel (**a**), the elongating injured blood vessel (**b**), and the sprouting blood vessel (**c**) during cutaneous wound angiogenesis at the timepoints indicated at the top. The merged images of *pdgfrb:mCherry* (red) and *kdrl:EGFP* (green) and the mCherry images (red). Arrowheads indicate the positions of PCs. The boxed areas in (**b**) are enlarged to the bottom. In (**a**), PCs covering the tortuous vessel divided into two daughter cells and moved in the opposite direction. In (**b**), PCs in the injured blood vessel divided during vessel repair. In (**c**), PCs located in the base of sprouting vessel migrated toward the tip and divided during vessel elongation. Scale bars: 50 μm (**a, e**)

of PDGF-B in ECs [39]. Therefore, PDGF-B released from activated ECs might regulate PC functions. Consistently, it has been reported that EC-derived platelet-derived growth factor (PDGF)-B induces proliferation and migration of PDGF receptor-β (PDGFRβ)-expressing mural cells during embryogenesis in mice [40]. A previous report also showed that PDGFRβ signaling is essential for PC recruitment during cutaneous wound healing [41]. Therefore, during cutaneous angiogenesis, ECs might be activated by VEGF to release PDGF-B, which in turn promotes proliferation and migration of PCs to cover the neovessels and tortuous vessels. This hypothesis will be confirmed by future study.

Macrophages are known to regulate various aspects of angiogenesis such as vessel sprouting, anastomosis, remodeling, and regression [26, 42–45]. Fantin et al. have previously reported that tissue macrophages bridge endothelial tip cells to promote their anastomosis during embryonic angiogenesis [43]. It has also been shown

that macrophages mediate the repair of brain vascular rupture through direct physical adhesion and mechanical traction [45]. In addition, Gurevich et al. have recently reported, by performing live imaging of angiogenesis in injured intersegmental vessels of zebrafish larvae, that pro-inflammatory macrophages associate with the tip of vessel sprouts and promote their elongation through VEGF secretion at the early stage of wound angiogenesis, while anti-inflammatory macrophages regulate vessel regression through induction of EC apoptosis and their phagocytosis at the late stage [26]. Therefore, it is important to elucidate the role of macrophages in cutaneous wound angiogenesis.

In conclusion, we live-imaged the complex and dynamic behavior of ECs and PCs during cutaneous angiogenesis in adult zebrafish. Cutaneous wound healing occurs through a complex and highly regulated mechanism which involves various types of cells, such as ECs and PCs as well as fibroblasts, inflammatory cells, and keratinocytes. Although we only visualized ECs and PCs to analyze cutaneous angiogenesis in this study, this live-imaging system can be used to image other types of cells such as fibroblasts, inflammatory cells, and keratinocytes. Therefore, this live-imaging system for adult zebrafish will be a valuable contribution to advance the field of wound healing research.

Acknowledgements We thank K. Kawakami (National Institute of Genetics) for the Tol2 system and D. Y. Stainier (Max Planck Institute for Heart and Lung Research) for *Tg(kdrl:EGFP)* and *Tg(gata1:DsRed)*. We are also grateful to E. Oguri-Nakamura, H. Ichimiya, S. Egawa, and K. Kato for excellent technical assistance. This work was supported in part by Grants-in-Aid for Scientific Research on Innovative Areas "Fluorescence Live imaging" (No. 22113009 to S.F.) of The Ministry of Education, Culture, Sports, Science, and Technology, Japan; by Grants-in-Aid for Scientific Research (B) (No. 25293050 to S.F.), for Exploratory Research (No. 17K19689 to S.F.), and for Scientific Research for Young Scientists (No. 17K15565 to S.Y.) from the Japan Society for the Promotion of Science; the Japan Agency for Medical Research and Development (AMED) under Grant Number JP17gm5810010 (to S.F.); the Core Research for Evolutional Science and Technology (CREST) program of Japan Science and Technology Agency (JST) (to N.M.); Takeda Science Foundation (to S.F.); the Naito Foundation (to S.F.); Daiichi Sankyo Foundation of Life Science (to S.F.) and Astellas Foundation for Research on Metabolic Disorders (to S.F.); and a research grant of the Princess Takamatsu Cancer Research Fund (to S.F.).

Author contributions CN, SY, and SF conceived and designed the research; CN, SY, and KA carried out experiments; YW generated *Tg(fli1a:mCherry)*^{ncv501} zebrafish line; CN and SY analyzed the data; NM and RO supported the study; SF wrote the manuscript.

Data availability The datasets generated during and/or analyzed during the current study are available from the corresponding author upon reasonable request.

Compliance with ethical standards

Conflict of interest The authors declare no competing interests.

References

1. Gurtner GC, Werner S, Barrandon Y, Longaker MT (2008) Wound repair and regeneration. Nature 453(7193):314–321. https://doi.org/10.1038/nature07039
2. Johnson KE, Wilgus TA (2014) Vascular endothelial growth factor and angiogenesis in the regulation of cutaneous wound repair. Adv Wound Care 3(10):647–661. https://doi.org/10.1089/wound.2013.0517
3. Richardson R, Slanchev K, Kraus C, Knyphausen P, Eming S, Hammerschmidt M (2013) Adult zebrafish as a model system for cutaneous wound-healing research. J Invest Dermatol 133(6):1655–1665
4. Carmeliet P (2005) Angiogenesis in life, disease and medicine. Nature 438(7070):932–936
5. Larrivee B, Freitas C, Suchting S, Brunet I, Eichmann A (2009) Guidance of vascular development. Circ Res 104(4):428–441
6. Chung AS, Ferrara N (2011) Developmental and pathological angiogenesis. Annu Rev Cell Dev Biol 27:563–584
7. Augustin HG, Koh GY, Thurston G, Alitalo K (2009) Control of vascular morphogenesis and homeostasis through the angiopoietin-Tie system. Nat Rev Mol Cell Biol 10(3):165–177
8. Brudno Y, Ennett-Shepard AB, Chen RR, Aizenberg M, Mooney DJ (2013) Enhancing microvascular formation and vessel maturation through temporal control over multiple pro-angiogenic and pro-maturation factors. Biomaterials 34(36):9201–9209. https://doi.org/10.1016/j.biomaterials.2013.08.007
9. Carmeliet P, Jain RK (2011) Molecular mechanisms and clinical applications of angiogenesis. Nature 473(7347):298–307. https://doi.org/10.1038/nature10144
10. Raza A, Franklin MJ, Dudek AZ (2010) Pericytes and vessel maturation during tumor angiogenesis and metastasis. Am J Hematol 85(8):593–598. https://doi.org/10.1002/ajh.21745
11. Sapieha P (2012) Eyeing central neurons in vascular growth and reparative angiogenesis. Blood 120(11):2182–2194. https://doi.org/10.1182/blood-2012-04-396846
12. Warmke N, Griffin KJ, Cubbon RM (2016) Pericytes in diabetes-associated vascular disease. J Diabetes Complicat 30(8):1643–1650. https://doi.org/10.1016/j.jdiacomp.2016.08.005
13. Gore AV, Monzo K, Cha YR, Pan W, Weinstein BM (2012) Vascular development in the zebrafish. Cold Spring Harb Perspect Med 2(5):a006684. https://doi.org/10.1101/cshperspect.a006684
14. Fukuhara S, Fukui H, Wakayama Y, Ando K, Nakajima H, Mochizuki N (2015) Looking back and moving forward: recent advances in understanding of cardiovascular development by imaging of zebrafish. Dev Growth Differ 57(4):333–340. https://doi.org/10.1111/dgd.12210
15. Fukuhara S, Zhang J, Yuge S, Ando K, Wakayama Y, Sakaue-Sawano A, Miyawaki A, Mochizuki N (2014) Visualizing the cell-cycle progression of endothelial cells in zebrafish. Dev Biol 393(1):10–23
16. Kawakami K, Takeda H, Kawakami N, Kobayashi M, Matsuda N, Mishina M (2004) A transposon-mediated gene trap approach identifies developmentally regulated genes in zebrafish. Dev Cell 7(1):133–144
17. Herbert SP, Huisken J, Kim TN, Feldman ME, Houseman BT, Wang RA, Shokat KM, Stainier DYR (2009) Arterial-venous segregation by selective cell sprouting: an alternative mode of blood vessel formation. Science 326(5950):294–298. https://doi.org/10.1126/science.1178577
18. Kwon HB, Fukuhara S, Asakawa K, Ando K, Kashiwada T, Kawakami K, Hibi M, Kwon YG, Kim KW, Alitalo K, Mochizuki N (2013) The parallel growth of motoneuron axons with the dorsal aorta depends on Vegfc/Vegfr3 signaling in zebrafish. Development 140(19):4081–4090

19. Ando K, Fukuhara S, Izumi N, Nakajima H, Fukui H, Kelsh RN, Mochizuki N (2016) Clarification of mural cell coverage of vascular endothelial cells by live imaging of zebrafish. Development 143(8):1328–1339. https://doi.org/10.1242/dev.132654
20. Xu C, Volkery S, Siekmann AF (2015) Intubation-based anesthesia for long-term time-lapse imaging of adult zebrafish. Nat Protoc 10(12):2064–2073
21. Chong DC, Yu Z, Brighton HE, Bear JE, Bautch VL (2017) Tortuous microvessels contribute to wound healing via sprouting angiogenesis. Arterioscler Thromb Vasc Biol 37(10):1903–1912. https://doi.org/10.1161/ATVBAHA.117.309993
22. Olson KR (1996) Secondary circulation in fish: anatomical organization and physiological significance. J Exp Zool 275:172–185
23. Rasmussen JP, Vo NT, Sagasti A (2018) Fish scales dictate the pattern of adult skin innervation and vascularization. Dev Cell 46(3):344–359 e344. https://doi.org/10.1016/j.devcel.2018.06.019
24. Yaniv K, Isogai S, Castranova D, Dye L, Hitomi J, Weinstein BM (2006) Live imaging of lymphatic development in the zebrafish. Nat Med 12(6):711–716. https://doi.org/10.1038/nm1427
25. Kuchler AM, Gjini E, Peterson-Maduro J, Cancilla B, Wolburg H, Schulte-Merker S (2006) Development of the zebrafish lymphatic system requires VEGFC signaling. Curr Biol 16(12):1244–1248. https://doi.org/10.1016/j.cub.2006.05.026
26. Gurevich DB, Severn CE, Twomey C, Greenhough A, Cash J, Toye AM, Mellor H, Martin P (2018) Live imaging of wound angiogenesis reveals macrophage orchestrated vessel sprouting and regression. EMBO J. https://doi.org/10.15252/embj.201797786
27. Rege A, Thakor NV, Rhie K, Pathak AP (2012) In vivo laser speckle imaging reveals microvascular remodeling and hemodynamic changes during wound healing angiogenesis. Angiogenesis 15(1):87–98. https://doi.org/10.1007/s10456-011-9245-x
28. Saaristo A, Veikkola T, Enholm B, Hytonen M, Arola J, Pajusola K, Turunen P, Jeltsch M, Karkkainen MJ, Kerjaschki D, Bueler H, Yla-Herttuala S, Alitalo K (2002) Adenoviral VEGF-C overexpression induces blood vessel enlargement, tortuosity, and leakiness but no sprouting angiogenesis in the skin or mucous membranes. FASEB J 16(9):1041–1049. https://doi.org/10.1096/fj.01-1042com
29. Urao N, Okonkwo UA, Fang MM, Zhuang ZW, Koh TJ, DiPietro LA (2016) MicroCT angiography detects vascular formation and regression in skin wound healing. Microvasc Res 106:57–66. https://doi.org/10.1016/j.mvr.2016.03.006
30. Armulik A, Genové G, Betsholtz C (2011) Pericytes: developmental, physiological, and pathological perspectives, problems, and promises. Dev Cell 21(2):193–215. https://doi.org/10.1016/j.devcel.2011.07.001
31. Sweeney MD, Ayyadurai S, Zlokovic BV (2016) Pericytes of the neurovascular unit: key functions and signaling pathways. Nat Neurosci 19(6):771–783
32. Hashizume H, Baluk P, Morikawa S, McLean JW, Thurston G, Roberge S, Jain RK, McDonald DM (2000) Openings between defective endothelial cells explain tumor vessel leakiness. Am J Pathol 156(4):1363–1380. https://doi.org/10.1016/s0002-9440(10)65006-7
33. Cogan DG, Toussaint D, Kuwabara T (1961) Retinal vascular patterns. IV. Diabetic retinopathy. Arch Ophthalmol 66(3):366–378
34. Frank RN (2004) Diabetic retinopathy. N Engl J Med 350(1):48–58. https://doi.org/10.1056/NEJMra021678
35. Uemura A, Ogawa M, Hirashima M, Fujiwara T, Koyama S, Takagi H, Honda Y, Wiegand SJ, Yancopoulos GD, Nishikawa S (2002) Recombinant angiopoietin-1 restores higher-order architecture of growing blood vessels in mice in the absence of mural cells. J Clin Investig 110(11):1619–1628. https://doi.org/10.1172/jci15621
36. Kim J, Chung M, Kim S, Jo DH, Kim JH, Jeon NL (2015) Engineering of a biomimetic pericyte-covered 3D microvascular network. PLoS ONE 10(7):e0133880. https://doi.org/10.1371/journal.pone.0133880
37. Eilken HM, Dieguez-Hurtado R, Schmidt I, Nakayama M, Jeong HW, Arf H, Adams S, Ferrara N, Adams RH (2017) Pericytes regulate VEGF-induced endothelial sprouting through VEGFR1. Nat Commun 8(1):1574. https://doi.org/10.1038/s41467-017-01738-3
38. Gerhardt H, Golding M, Fruttiger M, Ruhrberg C, Lundkvist A, Abramsson A, Jeltsch M, Mitchell C, Alitalo K, Shima D, Betsholtz C (2003) VEGF guides angiogenic sprouting utilizing endothelial tip cell filopodia. J Cell Biol 161(6):1163–1177
39. Kano MR, Morishita Y, Iwata C, Iwasaka S, Watabe T, Ouchi Y, Miyazono K, Miyazawa K (2005) VEGF-A and FGF-2 synergistically promote neoangiogenesis through enhancement of endogenous PDGF-B-PDGFRβ signaling. J Cell Sci 118(Pt 16):3759–3768. https://doi.org/10.1242/jcs.02483
40. Hellstrom M, Kalen M, Lindahl P, Abramsson A, Betsholtz C (1999) Role of PDGF-B and PDGFR-beta in recruitment of vascular smooth muscle cells and pericytes during embryonic blood vessel formation in the mouse. Development 126(14):3047–3055
41. Rajkumar VS, Shiwen X, Bostrom M, Leoni P, Muddle J, Ivarsson M, Gerdin B, Denton CP, Bou-Gharios G, Black CM, Abraham DJ (2006) Platelet-derived growth factor-β receptor activation is essential for fibroblast and pericyte recruitment during cutaneous wound healing. Am J Pathol 169(6):2254–2265. https://doi.org/10.2353/ajpath.2006.060196
42. Lobov IB, Rao S, Carroll TJ, Vallance JE, Ito M, Ondr JK, Kurup S, Glass DA, Patel MS, Shu W, Morrisey EE, McMahon AP, Karsenty G, Lang RA (2005) WNT7b mediates macrophage-induced programmed cell death in patterning of the vasculature. Nature 437(7057):417–421. https://doi.org/10.1038/nature03928
43. Fantin A, Vieira JM, Gestri G, Denti L, Schwarz Q, Prykhozhij S, Peri F, Wilson SW, Ruhrberg C (2010) Tissue macrophages act as cellular chaperones for vascular anastomosis downstream of VEGF-mediated endothelial tip cell induction. Blood 116(5):829–840. https://doi.org/10.1182/blood-2009-12-257832
44. Rymo SF, Gerhardt H, Wolfhagen Sand F, Lang R, Uv A, Betsholtz C (2011) A two-way communication between microglial cells and angiogenic sprouts regulates angiogenesis in aortic ring cultures. PLoS ONE 6(1):e15846. https://doi.org/10.1371/journal.pone.0015846
45. Liu C, Wu C, Yang Q, Gao J, Li L, Yang D, Luo L (2016) Macrophages mediate the repair of brain vascular rupture through direct physical adhesion and mechanical traction. Immunity 44(5):1162–1176. https://doi.org/10.1016/j.immuni.2016.03.008